Magnetic and electrical properties of the ternary compound $U_2Ir_3Si_5$ with one-dimensional uranium zigzag chains

D. X. Li,[1] F. Honda,[1] A. Miyake,[2] Y. Homma,[1] Y. Haga,[3] A. Nakamura,[1] Y. Shimizu,[1] A. Maurya,[1] Y. J. Sato,[1] M. Tokunaga,[2] and D. Aoki[1]

[1]*Institute for Materials Research, Tohoku University, Oarai, Ibaraki 311-1313, Japan*
[2]*Institute for Solid State Physics, The University of Tokyo, Kashiwa, Chiba 277-8581, Japan*
[3]*Advanced Science Research Center, Japan Atomic Energy Agency, Tokai, Ibaraki 319-1195, Japan*

(Received 14 November 2018; published 8 February 2019)

The physical properties of the single-crystalline $U_2Ir_3Si_5$, a new ternary uranium compound with $U_2Co_3Si_5$-type orthorhombic structure, are investigated by means of magnetic susceptibility $\chi(T)$, specific heat $C(T)$, electrical resistivity $\rho(T)$, and high-field magnetization $M(H,T)$ measurements. $U_2Ir_3Si_5$ undergoes an antiferromagnetic transition at $T_N = 36$ K followed by a first-order phase transition at $T_0 = 25.5$ K. The sharp peak in $C(T)$ at T_0 and the obvious hysteresis behavior in $\chi(T)$, $\rho(T)$, and $M(H,T)$ around T_0 provide strong evidence for the first-order phase transition. The $\rho(T)$ measurements along the a and b axes reveal the negative temperature coefficients of resistance over a wide temperature range, which can be understood based on the semiconductorlike narrow band gap model or the Kondo effect. The $M(H)$ curve measured at 4.2 K along the b axis shows three-step metamagnetic transitions within a narrow field region around 200 kOe and a large hysteresis near the first transition field, while the $M_{H\|a}(H)$ and $M_{H\|c}(H)$ curves show no transitions up to 560 kOe suggesting the strong magnetic anisotropy. A possible mechanism of the first-order phase transition at T_0 is the occurrence of a magnetic quadrupolar order, resulting from the quasi-one-dimensional uranium zigzag chain.

DOI: 10.1103/PhysRevB.99.054408

I. INTRODUCTION

The ternary intermetallics $R_2M_3X_5$ (R = rare earth or actinide, M = transition metals and X = Si, Ge and Sn, referred to herein as "235" compounds) form a large family among the rare earth and actinide based compounds. The crystal structure of most "235" compounds belongs to one of the following four types, i.e., orthorhombic $U_2Co_3Si_5$-type with space group $Ibam$, monoclinic $Lu_2Co_3Si_5$-type with space group $C2/c$, tetragonal $Sc_2Fe_3Si_5$-type with space group $P4/mnc$, and orthorhombic $Y_2Rh_3Sn_5$-type with space group $Cmc2_1$. In recent years, great interest has been devoted to the compounds of this family due to their wide variety of electronic properties. The typical examples include the first-order antiferromagnetic (AFM) transition in $U_2Rh_3Si_5$ [1], high magnetoresistance in $Pr_2Ni_3Ge_5$ [2], crystalline electric field (CEF) effects in $Ce_2Pt_3Si_5$ [3], Kondo-lattice behavior in $Ce_2Rh_3Ge_5$ and $Ce_2Ir_3Ge_5$ [4], valence fluctuation in $Ce_2Co_3Ge_5$ [5], multiple charge-density-wave (CDW) transitions in $Lu_2Ir_3Si_5$ [6], pressure-induced heavy-fermion superconductivity in $Ce_2Ni_3Ge_5$ [7], AFM superconductivity behavior in $Pr_2Pt_3Ge_5$ [8], pressure-induced superconductivity in $Tm_2Fe_3Si_5$ [9], field-induced metamagnetic transition (MMT) in $Pr_2Pd_3Ge_5$ [10], ferromagnetic (FM) transition with localized $5f$ moments in $Pu_2Pt_3Si_5$ [11], and complex magnetic ordering with enhanced Sommerfeld coefficient in $Pu_2Ni_3Si_5$ and $Pu_2Co_3Si_5$ [12].

Considering the possible dual nature of $5f$ electrons, we are particularly interested in the physical properties of uranium based compounds among the $R_2M_3X_5$ family. Relative to the study of rare-earth "235" compounds, however, research on uranium "235" systems is rare. Up to now, magnetic property and/or crystal structure of uranium "235" systems have been reported only for several silicides, they are $U_2M_3Si_5$ with M = Fe [13], Ru [13–15], Rh [13,15], Os [13], Co [15], Mn [16], Tc [17], and Re [18]. Except for $U_2Co_3Si_5$ that crystallizes in the orthorhombic structure with space group $Ibam$, the first four compounds and the last three compounds have been confirmed to crystallize in the monoclinic $Lu_2Co_3Si_5$-type structure (space group $C2/c$) and the tetragonal $Sc_2Fe_3Si_5$-type structure (space group $P4/mnc$), respectively. Among them, two systems, $U_2Rh_3Si_5$ and $U_2Tc_3Si_5$, are found to exhibit long-range AFM order with the transition temperature $T_N = 25$ and 11 K, respectively. Of particular note is that physical properties of single-crystalline U-based "235" compounds have been reported only for $U_2Rh_3Si_5$, which shows fascinating magnetic natures including the first-order AFM phase transition, and the high MMT field with a remarkable magnetic anisotropy [1,19–21]. Obviously, research on physical properties of "235" compounds to date is far from comprehensive. In order to systematically understand the variety of physical properties in these compounds, further investigations on other members of this family, particularly on U-based systems, are strongly desired and seem to be very interesting (considering their unique crystal structures such as zigzag chain of U atoms). We have verified the existence of single phase compound $U_2Ir_3Si_5$, a new member of the "235" family, and successfully grown its high quality single crystal. The preliminary data of physical property measurements were briefly reported in a conference proceedings [22], but it was then found that the determined crystal axis directions were incorrect. In this paper, we present the detailed fundamental

physical property measurements of the $U_2Ir_3Si_5$ single crystal after axial correction including the temperature and magnetic field dependences of susceptibility, specific heat, electrical resistivity, and high-field magnetization. The obtained results are discussed by comparing with the data reported for $U_2Rh_3Si_5$ as well as other "235" compounds.

II. EXPERIMENT DETAILS

The $U_2Ir_3Si_5$ single crystal was grown by the Czochralski method in a tetra-arc furnace. Purities of the starting materials are 99.9% (3N purity) for U, 4N for Ir, and 6N for Si. The single-crystal x-ray diffraction data was collected on a Rigaku XtaLAB mini diffractometer with Mo $K\alpha$ radiation and solved with the direct method using the SHELXT program. Furthermore, the powder x-ray diffraction method and the x-ray Laue intensified CCD camera technique were used to characterize the quality of the crystal and to determine the crystalline orientation. Because the homogeneity of the $U_2Ir_3Si_5$ single crystal was found to deteriorate after annealing at 900 °C for one week, the small single crystals (cut from a large crystal by using a spark cutter) in their "as-cast" forms are chosen for use in this work. Magnetic susceptibility and low-field magnetization were measured at temperatures down to 2 K and at magnetic fields up to 55 kOe by using a superconducting quantum interference device (SQUID, Quantum Design) magnetometer. The thermal-relaxation technique was employed for specific-heat measurements in the temperature range between 0.4 and 49 K by using a physical properties measurement system (PPMS, Quantum Design). Electrical resistivity between 1.8 and 300 K was measured using a standard four-terminal ac method. High-field magnetization measurements up to 560 kOe were performed at the International MegaGauss Science Laboratory of the Institute for Solid State Physics, the University of Tokyo, by the standard induction method using coaxial pickup coils in a pulsed field magnet.

III. RESULTS

Tables I and II list the crystallographic and structure refinement results, atomic positions, and equivalent isotropic thermal displacement parameters of $U_2Ir_3Si_5$, which are determined by solving the single-crystal x-ray diffraction data. The refinement results indicate that $U_2Ir_3Si_5$ crystallizes with the orthorhombic $U_2Co_3Si_5$-type structure (space group *Ibam*) with the lattice parameters $a = 9.9467(6)$ Å, $b = 11.3022(6)$ Å, and $c = 5.8719(3)$ Å. The crystal structure of $U_2Ir_3Si_5$ is shown in Fig. 1. In this structure, the U, Ir, and Si atoms occupy one, two, and three kinds of lattice sites, respectively, i.e., 8j site for U, 4a and 8j sites for Ir, 4b, 8g, and 8j sites for Si. The shortest U-U distance is 4.0066(3) Å. Linking these nearest neighbor U atoms as illustrated in Fig. 1 can form a quasi-one-dimensional (1D) zigzag chain along the c axis, which is well separated from the Ir-Si ring, while the Ir-Si-Ir bond is formed as a cage around the U atoms on the quasi-1D zigzag chain. Detailed discussion on the $U_2Co_3Si_5$-type crystal structure can be found in the literatures (e.g., Refs. [6,12]). Using the crystallographic parameters listed in Tables I and II the powder x-ray diffraction spectrum of $U_2Ir_3Si_5$ is calculated and is shown in Fig. 2(a) together with the experimental result. Comparing the experimental and calculated patterns, no impurity phase is observed. In addition, the Laue photograph obtained for the [001] axis [Fig. 2(b)] shows almost no splitting of the Laue spots. These results indicate a high quality of the $U_2Ir_3Si_5$ single crystal.

TABLE I. Crystallographic and structure refinement data for $U_2Ir_3Si_5$.

Compound	$U_2Ir_3Si_5$
Crystal system	Orthorhombic
Space group	*Ibam* (#72)
Lattice parameters	$a = 9.9467(6)$ Å
	$b = 11.3022(6)$ Å
	$c = 5.8719(3)$ Å
	$V = 660.12(6)$ Å^3
Formula weight	1193.15
Calculated density	12.005 g cm^{-3}
F(000)	1940
No. of reflections measured	1346
	unique: 621($R_{\rm int} = 0.0730$)
Refinement method	Full-matrix least squares on F^2
$R1$ ($I > 2.00\sigma(I)$)	0.0458
R (All reflections)	0.0488
$wR2$ (All reflections)	0.1222
Goodness of fit	1.192

The temperature (T) dependences of magnetization (M) of $U_2Ir_3Si_5$ are measured in various magnetic field (H) applied along the a, b, and c axes, respectively. For convenience, hereafter, we call M/H dc susceptibility and denote it as χ. The experimental results measured with zero-field cooling (ZFC) and field cooling (FC) processes show no significant difference between the $\chi_{\rm ZFC}(T)$ and $\chi_{\rm FC}(T)$ curves for the three crystallographic axis directions even in a small applied field. Figure 3 presents the susceptibility and the reciprocal susceptibility data measured in a field of 500 Oe. At high temperatures ($T > 90$ K), the $\chi_{H\|b}(T)$ and $\chi_{H\|a}(T)$ behaviors can be fitted using the modified Curie-Weiss law $\chi(T) = \chi_0 + C/(T - \Theta_P)$, where C is the Curie constant, Θ_P the paramagnetic Curie temperature, and χ_0 denotes temperature-independent contributions such as core diamagnetism, Landau diamagnetism, and Pauli paramagnetism [see the solid lines of Fig. 3(b)]. For $H \parallel b$, the effective magnetic moment $\mu_{\rm eff}$ estimated from the fitting is 3.6 μ_B/U as expected for a free U ion with an f^2 or f^3 electronic configuration, while a negative paramagnetic Curie temperature $\Theta_P = -11$ K is obtained characterizing the nature of an antiferromagnet, whereas the

TABLE II. Atomic positions and equivalent isotropic thermal displacement parameters for $U_2Ir_3Si_5$.

Atom	Site	x	y	z	B_{eq}
U	8j	0.27070(7)	0.13077(5)	0	0.11(2)
Ir1	4a	0	0	0.25	0.16(2)
Ir2	8j	0.11544(7)	0.36086(6)	0	0.08(2)
Si1	4b	0.5	0	0.25	0.09(10)
Si2	8g	0	0.2280(5)	0.25	0.15(7)
Si3	8j	0.3471(5)	0.3910(5)	0	0.24(7)

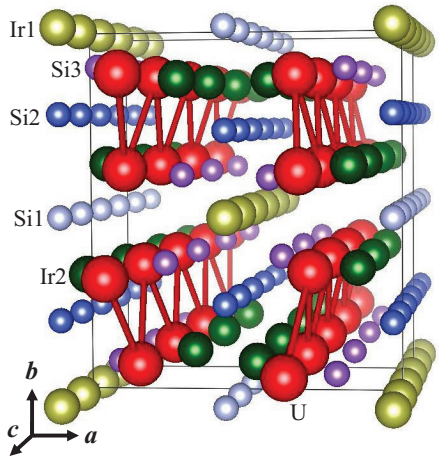

FIG. 1. The crystal structure of $U_2Ir_3Si_5$.

corresponding values obtained for $H \parallel a$ are $\mu_{\text{eff}} = 2.1\ \mu_B$/U and $\Theta_P = -62.9$ K. The larger and negative Θ_P value suggests much stronger AFM exchange interaction in the a-axis direction. In the case of $H \parallel c$, however, the $\chi_{H\parallel c}(T)$ curve shows a small and broad peak centered at ~150 K, and this

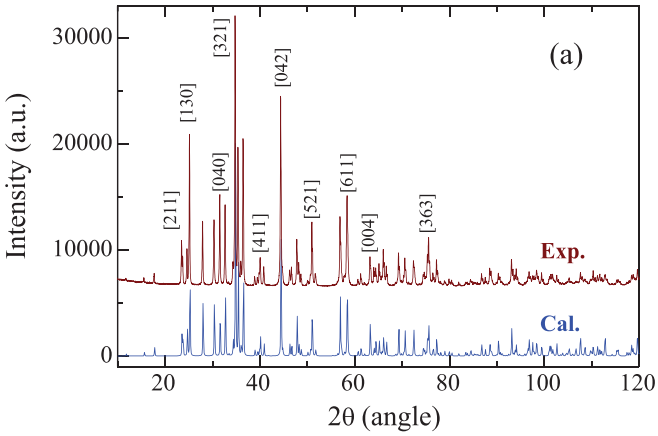

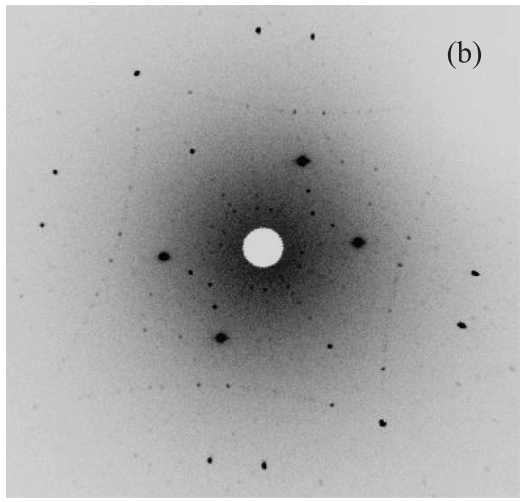

FIG. 2. (a) Experimental and calculated results of powder x-ray diffraction of the pulverized $U_2Ir_3Si_5$ single crystal at room temperature. (b) The Laue pattern of $U_2Ir_3Si_5$ for the (001) plane.

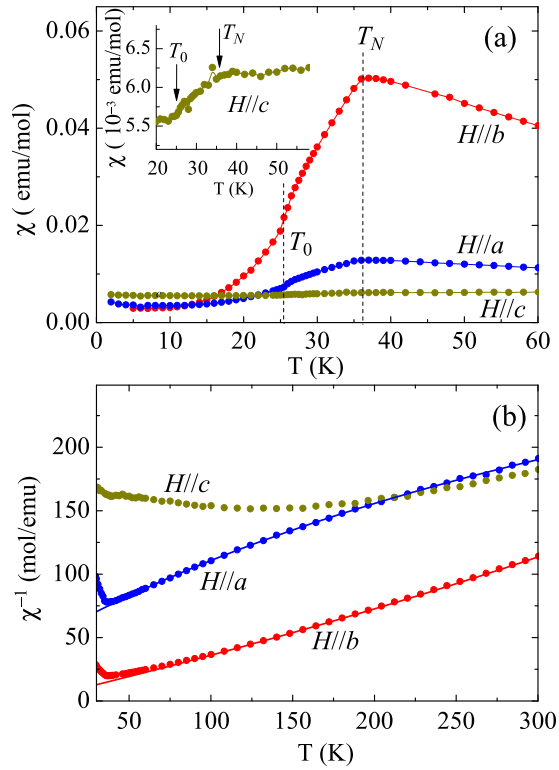

FIG. 3. Temperature dependences of ZFC susceptibility ($\chi = M/H$) (a), and inverse susceptibility (b) of single crystalline $U_2Ir_3Si_5$ in a magnetic field of 500 Oe for $H \parallel a$, $H \parallel b$, and $H \parallel c$. The inset of panel (a) shows the expanded plot of $\chi_{H\parallel c}(T)$ curve. The solid lines in panel (b) display the fitting results of $\chi_{H\parallel b}(T)$ and $\chi_{H\parallel a}(T)$ using the modified Curie-Weiss law (see the text).

fitting does not give physically meaningful values of μ_{eff} and Θ_P indicating the more complex magnetic behavior. These different magnetic susceptibility behaviors reflect significant magnetocrystalline anisotropy. Moreover, if we fit the data above ~230 K using the same modified Curie-Weiss law, the estimated μ_{eff} value (~3.5 μ_B/U) is almost no difference for $H \parallel a$ and $H \parallel b$.

At low-temperature side [see Fig. 3(a)], the important findings are the strong magnetic anisotropy and the double phase transitions. In the case of $H \parallel b$, a large peak appears at the temperature $T_N = 36$ K representing the magnetic phase transition from high-temperature paramagnetic (PM) state to low-temperature AFM state. For $H \parallel a$ and $H \parallel c$, this PM-AFM transition can also be detected at T_N in $\chi_{H\parallel a}(T)$ and $\chi_{H\parallel c}(T)$ curve, respectively, marked by a relatively small peak [also see the inset of Fig. 3(a)]. It is interesting to note that as the temperature is further decreased down to $T_0 \sim 25.5$ K, the susceptibility curve shows a sharp drop. This phenomenon is most significant for $H \parallel b$, which displays the obvious characteristics of first-order phase transition as described below.

Figure 4 illustrates the temperature dependences of magnetization of $U_2Ir_3Si_5$ measured near the transition temperatures T_N and T_0 in various magnetic fields between 0.5 and 55 kOe applied along the a, b, and c axes. The double phase transitions can be more clearly observed from this figure. For the

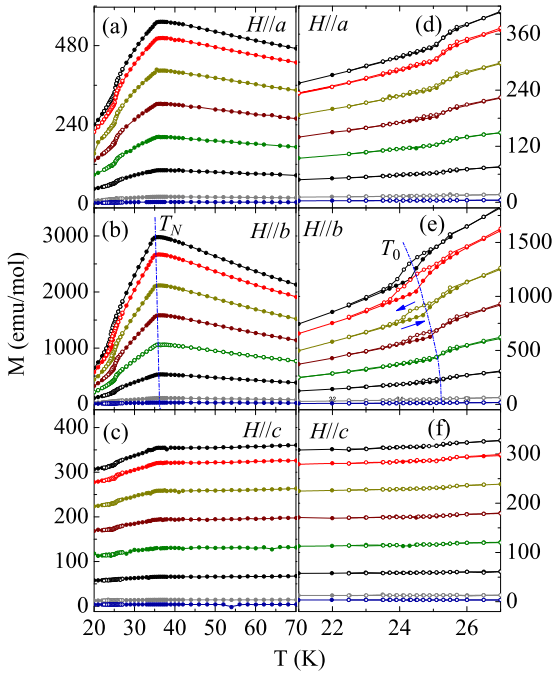

FIG. 4. (a)–(c) Low temperature ZFC susceptibility of single crystalline $U_2Ir_3Si_5$ measured in magnetic fields of 55, 50, 40, 30, 20, 10, 2, and 0.5 kOe (curve from top to bottom) for $H \parallel a$, $H \parallel b$, and $H \parallel c$, respectively. (d)–(f) The expanded plot of the susceptibility around the transition temperature T_0 measured in magnetic fields of 55, 50, 40, 30, 20, 10, 2, and 0.5 kOe (curve from top to bottom) for $H \parallel a$, $H \parallel b$, and $H \parallel c$, respectively. The dotted lines in (b) and (e) are drawn to guide the eye.

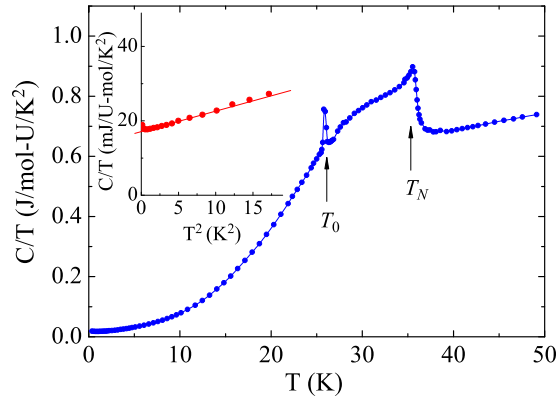

FIG. 5. Temperature dependence of specific heat $C(T)$ of single crystalline $U_2Ir_3Si_5$ plotted as C/T vs T down to 0.4 K. The inset shows the plot of C/T vs T^2 at low temperatures.

three crystallographic axis directions, the peak temperature T_N shows a very small change as H increases to 55 kOe. In the case of $H \parallel b$, for example, T_N shifts from 36 K in 0.5 kOe to 35.2 K in 55 kOe [Fig. 4(b)]. Under the same field change, the field dependences of T_N for $H \parallel a$ and $H \parallel c$ are much smaller than that for $H \parallel b$ [Fig. 4(a) and 4(c)]. In addition, another transition temperature T_0 that is defined as the point where $M(T)$ curve begins to turn sharply upwards with increasing T, shows a similar small decrease when H increases from 0.5 kOe to 55 kOe. What should be emphasized here is that thermal hysteresis effect can be clearly observed in the $M(T)$ curves around T_0 at higher magnetic fields, specifically in the case of $H \parallel b$ [Fig. 4(e)], strongly evidencing the first-order nature of this transition. Note that the thermal hysteresis effect appearing in the $M(T)$ curves around T_0 is weak for $H \parallel a$ [Fig. 4(d)] and almost cannot be detected for $H \parallel c$ [Fig. 4(f)].

The double phase transitions at T_N and T_0 in $U_2Ir_3Si_5$ are also observed in the specific-heat measurement. As shown in Fig. 5, the temperature dependence of specific heat [plotted as $C(T)/T$ vs T] measured down to 0.4 K reveals two evident peaks. The high-temperature side peak appearing near $T_N =$ 36 K corresponds to the PM-AFM transition, while the small but very sharp peak appearing at T_0 has the characteristic of a first-order phase transition. These results are consistent with the magnetic susceptibility (Fig. 4) and electrical-resistivity measurements as described later. Because there is no suitable specific-heat data of a nonmagnetic reference material, the lattice contribution to the specific heat cannot be determined correctly, therefore we cannot estimate the value of magnetic entropy near the transition temperature T_N at this stage. On the other hand, the C/T vs T^2 plot shown in the inset of Fig. 5 yields for $T \to 0$ a value for the specific-heat coefficient of the T-linear term, $\gamma = 17$ mJ (mole U)$^{-1}$ K^{-2}. This value is comparable to that observed for $U_2Rh_3Si_5$ [1] and significantly less than that reported for the general heavy-fermion compound.

The electrical resistivity versus temperature, $\rho(T)$, is shown in Fig. 6. At room temperature, relatively large resistivity with the values of $\rho_{I\parallel a}(T) = 556\ \mu\Omega$ cm, $\rho_{I\parallel b}(T) =$ $486\ \mu\Omega$ cm, and $\rho_{I\parallel c}(T) = 214\ \mu\Omega$ cm are observed. As decreasing T from room temperature down to the AFM transition temperature, the change in the absolute value of the resistivity is small regardless of the direction of the current. The resistivity ratios between 300 and 36 K(T_N) are $\rho(300\ \text{K})/\rho(T_N) = 0.81$, 0.87 and 0.99 for $I \parallel a$, $I \parallel b$, and $I \parallel c$, respectively. Moreover, the temperature coefficient of resistance (TCR), defined as $\mathrm{d}\rho/dT$, is negative for $I \parallel a$ and $I \parallel b$, while the $\rho_{I\parallel c}(T)$ curve reveals a small and very broad peak centered at 160 K [see the inset of Fig. 6(a)]. Note that similar resistivity properties, i.e., very weak temperature dependence and negative TCR behavior have been observed in both polycrystalline (Fig. 3 in Ref. [23]) and single crystalline (Fig. 4 in Ref. [1]) $U_2Rh_3Si_5$ at high temperatures ($>T_N$). It is considered that $U_2Rh_3Si_5$ is not a heavy-fermion system [1].

At low-T side, all the $\rho_{I\parallel a}(T)$, $\rho_{I\parallel b}(T)$, and $\rho_{I\parallel c}(T)$ curves show a sharp rise as T decreases to T_N and T_0, then continue to extend up to about 5 K, and finally tend to saturate near 1.8 K, the lowest temperature measured. As illustrated in Fig. 6(b), another important phenomenon worthy of attention is the thermal hysteresis behavior that can be clearly observed in $\rho(T)$ curves around T_0 for all three current directions, i.e., $I \parallel a$, $I \parallel b$, and $I \parallel c$, even at zero field. This result also strongly demonstrates the first-order nature of the phase transition at T_0.

In Fig. 7 the field and temperature dependences of magnetization of $U_2Ir_3Si_5$, measured in magnetic field up to 55 kOe applied along the three principal crystallographic directions, are displayed. The anisotropic behavior of the $M(H)$ curves can also be found from this figure. First, for $H \parallel a$ and $H \parallel c$,

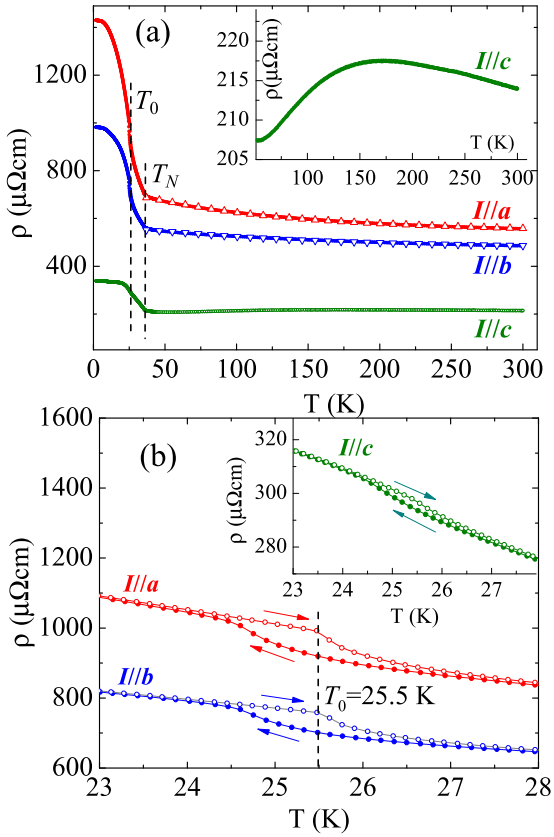

FIG. 6. (a) Temperature dependences of electrical resistivity of single crystalline $U_2Ir_3Si_5$ for measuring current parallel a, b, and c axes ($I \parallel a$, $I \parallel b$, and $I \parallel c$). The open triangle symbols represent the results of the least-square fits of the experimental data between 38 and 300 K to Eq. (1) for $I \parallel a$ (up triangle) and $I \parallel b$ (down triangle). Inset of (a): Expanded plot of the electrical resistivity in the high temperature region for $I \parallel c$. (b) Expanded plot of the electrical resistivity around the transition temperature $T_0 = 25.5$ K for $I \parallel a$ and $I \parallel b$. Inset of (b): Expanded plot of the electrical resistivity around transition temperature $T_0 = 25.5$ K for $I \parallel c$.

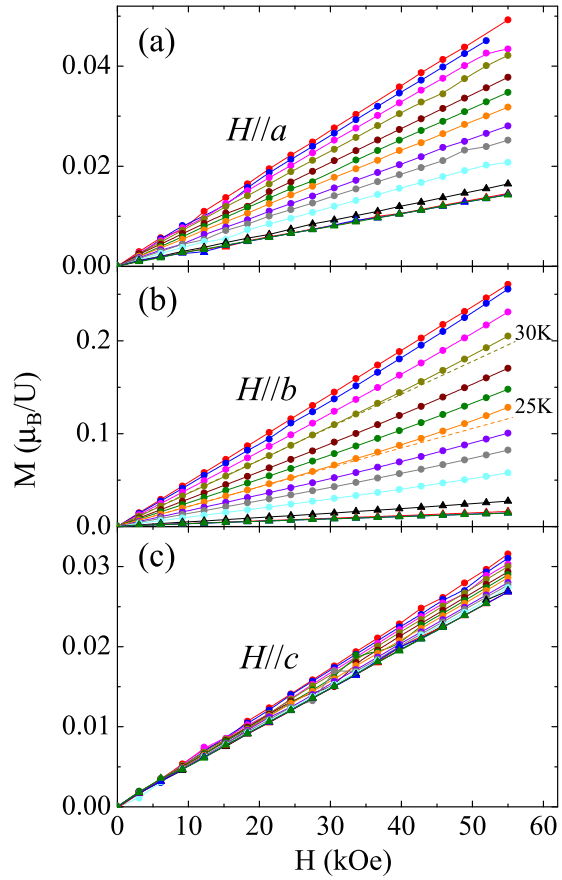

FIG. 7. (a)–(c) Magnetization of single crystalline $U_2Ir_3Si_5$ measured between 0 and 55 kOe at temperatures of 40, 34, 32, 30, 27.5, 26, 25, 24, 22.5, 20, 15, 10, 5, and 2 K (curve from top to bottom) for $H \parallel a$, $H \parallel b$, and $H \parallel c$, respectively. The two dotted straight lines in (b) are drawn to guide the eye.

$M(H)$ changes almost linearly with H up to 55 kOe in the temperature range between 2 and 40 K. In the case of $H \parallel b$, however, such a linear behavior appears at the temperatures far from the AFM phase transition point T_N, and the $M(H)$ curve measured around T_N begins to bend upward near 55 kOe. Second, in a fixed magnetic field, $M_{H\parallel b}$ changes most significantly with temperature comparing to $M_{H\parallel a}$ and $M_{H\parallel c}$. The $M_{H\parallel b}$ value in $H = 55$ kOe changes from 0.015 μ_B/U at 2 K to 0.26 μ_B/U at 40 K, that is, the rate of change of magnetization $[M(40\ \text{K})–M(2\ \text{K})]/M(2\ \text{K})|_{H=55\text{kOe}} = 16.9$. The corresponding value is 2.45 for $H \parallel a$ and only 0.18 for $H \parallel c$. On the other hand, the $M(H)$ value at $T = 2$ K is very small, even for $H \parallel b$ $M(H)$ only reaches to 0.015 μ_B/U as H rises to 55 kOe. This value is much smaller than the expected spontaneous magnetization for U^{3+} or U^{4+} ion, suggesting the possible MMT from AFM state to the polarized state at higher magnetic field. The high-field magnetization measurements described below have verified this possibility.

Figure 8(a) shows the high-field magnetization of $U_2Ir_3Si_5$ up to 370 kOe measured with rising H along the b axis at various temperatures. At 4.2 K, $M(H)$ increases linearly with field up to about 170 kOe; here, a small magnetic moment of 0.12 μ_B/U is induced. By further increasing H, the $M(H)$ curve shows three successive sharp jumps within about 20 kOe that occur at $H_1 = 195$ kOe, $H_2 = 201$ kOe, and $H_3 = 216$ kOe, respectively [see the inset of Fig. 8(a)]. Above ~220 kOe, $M(H)$ slowly increases with increasing H and reaches a value of 1.9 μ_B/U at 370 kOe. At the first, second, and third jump, the $M(H)$ value switches to a value of about 0.80, 1.33, and 1.82 μ_B/U, which is about 42%, 70%, and 96% of the $M(H)$ value at 370 kOe, respectively. In addition, a large hysteresis behavior with a width of ~20 kOe is observed in the $M(H)$ curve by sweeping the field up or down through the transition field H_1 [inset of Fig. 8(a)], indicating the first-order nature of this transition, which is consistent with susceptibility and resistivity measurements. On the other hand, both $M_{H\parallel a}(H)$ and $M_{H\parallel c}(H)$ measured at 4.2 K reveal almost H-linear behaviors up to 560 kOe. The data up to 400 kOe are also illustrated in Fig. 8(a) for comparison. At 560 kOe, small induced moments of $M_{H\parallel a} \approx 0.2$ μ_B/U and $M_{H\parallel c} \approx 0.24$ μ_B/U are detected suggesting that MMT's may occur under much higher magnetic fields along these two directions.

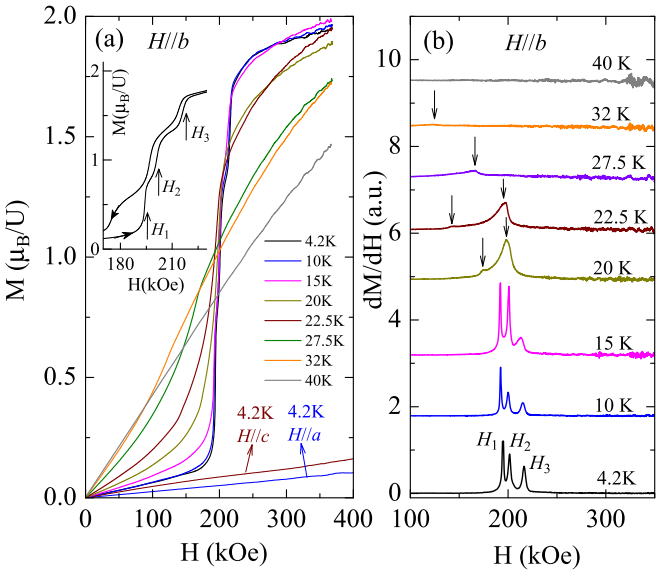

FIG. 8. (a) High-field magnetization $M(H)$ of single crystalline $U_2Ir_3Si_5$ measured at various temperatures for $H \parallel b$ and at 4.2 K for $H \parallel a$ and $H \parallel c$ (field sweep up). Inset of (a): Expanded plot of the $M_{H\parallel b}(H)$ curve near $H \sim 200$ kOe measured at $T = 4.2$ K, which shows clear metamagnetic transition and hysteresis behavior. (b) The field derivative, dM/dH, in the field range 100–350 kOe for $H \parallel b$.

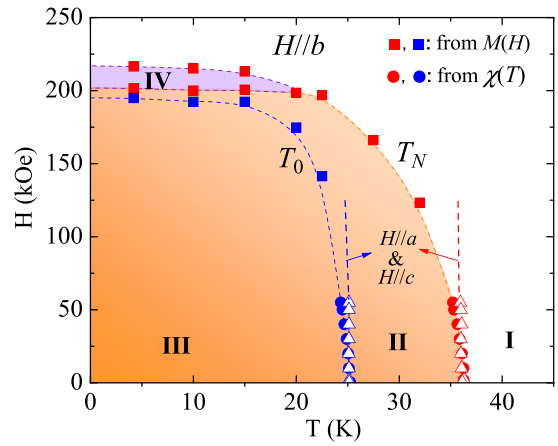

FIG. 9. The magnetic phase diagram of $U_2Ir_3Si_5$. The data were obtained by high-field magnetization (solid square: $H \parallel b$) and dc-SQUID susceptibility (solid circle: $H \parallel b$; open triangle: $H \parallel a$ and $H \parallel c$) measurements.

The high-field magnetization measurements mentioned above clearly demonstrate the presence of strong magnetic anisotropy in $U_2Ir_3Si_5$ with easy magnetic axis oriented along the crystallographic b axis. Similar anisotropic high-field magnetic behavior has been observed also for $U_2Rh_3Si_5$, which shows the MMT marked by a sharp jump in $M_{H\parallel b}(H)$ curve at 114 kOe and H-linear behavior in $M_{H\parallel a'}(H)$ and $M_{H\parallel c}(H)$ curves up to 300 kOe [20]. However, corresponding to the multistep MMT's in $M_{H\parallel b}(H)$ curve observed for $U_2Ir_3Si_5$, only a single large jump is detected in the $M_{H\parallel b}(H)$ curve for $U_2Rh_3Si_5$, suggesting a more complex magnetic structure in $U_2Ir_3Si_5$.

The field derivative of the magnetization measured for $H \parallel b$ [Fig. 8(a)] is displayed in Fig. 8(b) as a function of H. The three sharp jumps appearing in low-temperature $M(H)$ curves [inset of Fig. 8(a)] are clearly reflected in the three peaks at H_1, H_2, and H_3 marking the metamagnetic transition points. It is evident from this figure that three distinct peaks can be observed in the dM/dH curves below 15 K, and the peak positions shift slightly to lower fields with increasing T. Between 20 and 22.5 K, there are still two peaks that can be observed and began to move rapidly toward the low field with increasing T. Further raising the temperature, only one small peak can be detected between 27.5 and 32 K, which moves faster to the low field with increasing T.

The H-T phase diagram of $U_2Ir_3Si_5$ obtained from the magnetic susceptibility and high-field magnetization measurements is illustrated in Fig. 9. Along the b axis, three-step, two-step, and one-step transition fields can be found in the temperature ranges $T < 15$ K, $20 < T < 25$ K, and $25 < T < 36.3$ K, respectively, with the possible phase boundaries shown by the dashed lines in this figure. The I-II phase transition represents that the spin structure changes from a PM arrangement to an AFM one. The II-IV phase transition may be caused by some kind of spin reorientation. With respect to the II-III first-order phase transition, it seems to be due to structural variation accompanied by a possible quadrupolar ordering, which will be discussed further in the next section. In addition, no field transitions are detected along the a and c axes up to 560 kOe.

IV. DISCUSSION

The experimental results described above demonstrate that $U_2Ir_3Si_5$ shows anomalous magnetic and electrical properties. We are particularly interested in the negative TCR, i.e., $d\rho/dT$ and the first-order phase transition. It is well known that negative TCR over a wide range of temperature is a common phenomenon for structurally and/or chemically disordered systems [24,25]. The compound $U_2Ir_3Si_5$, however, possesses a perfectly ordered crystal structure, therefore the unusual negative TCR observed in this system deserves attention. As discussed in detail by Pandey *et al.* [26], the frequently appointed mechanisms suitable for highly disordered systems, such as the Ziman model [27] and the incipient localization [28] etc., cannot be used to explain the negative TCR observed for $U_2Ir_3Si_5$ in this work. In addition, because $U_2Ir_3Si_5$ exhibits clear AFM ordering at low temperature and the modified Curie-Weiss paramagnetic behavior at high temperature, the Baym-Meisel-Cote theory applicable only to nonmagnetic amorphous compounds with weak Pauli paramagnetism [26,29,30] is also not appropriate for use here. One possible explanation for the negative TCR observed in $U_2Ir_3Si_5$ above T_N can be based on the semiconductorlike narrow band gap model [31–33]. Indeed, in the temperature range of 38–300 K, $\rho_{I\parallel a}(T)$ and $\rho_{I\parallel b}(T)$ can be well approximated by the formula

$$\frac{1}{\rho(T)} = \alpha + \beta \exp\left(\frac{-E_g}{2k_BT}\right) \quad (1)$$

which represents the scattering of conduction electrons excited over the energy gap E_g. The best results obtained by least-squares fitting of this equation to the experimental data are shown by the open triangles in Fig. 6(a). This fitting yields the values of parameters $\alpha = 1.4 \times 10^{-3}$ $(\mu\Omega\,\mathrm{cm})^{-1}$, $\beta = 5.248 \times 10^{-4}$ $(\mu\Omega\,\mathrm{cm})^{-1}$, and $E_g = 19.4$ meV for $I \parallel a$, and $\alpha = 1.8 \times 10^{-3}$ $(\mu\Omega\,\mathrm{cm})^{-1}$, $\beta = 4.0 \times 10^{-4}$ $(\mu\Omega\,\mathrm{cm})^{-1}$, and $E_g = 22.7$ meV for $I \parallel b$. Similar semiconductorlike resistivity behavior in the paramagnetic states has been reported for crystalline compounds RNiSb (R = Tb and Ho) [34], RPdSb (R = Er and Y) [32], and RPdBi (R = Dy and Ho) [31]. As for the broad peak seen in $\rho_{I\|c}(T)$ curve [inset of Fig. 6(a)], it may be due to other additional influences, such as the relatively strong hybridization between the $5f$ and conduction electrons in the c-axis direction. Note that a broad peak is also observed in the $\chi_{H\|c}(T)$ curve (see Fig. 3) around similar temperatures, which may be originated from the same mechanism.

On the other hand, considering the observed small γ value ($\sim$17 mJ K^{-2} mol^{-1}, see Fig. 5), the low-T entropy of $5f$ electrons seems to be exhausted mostly by the occurrence of double phase transitions at T_N and T_0. In such a case, the low-T excitations of heavy quasiparticles formed by the Kondo effect are considered to be very weak. Nevertheless, the Fermi surface in the paramagnetic region should be different from that in the ordered states, thus we could not deny the possible existence of the Kondo effect, which could also lead to the negative TCR behavior.

As often observed in antiferromagnet, the sharp rise of $\rho_{I\|a}(T)$, $\rho_{I\|b}(T)$, and $\rho_{I\|c}(T)$ just below T_N and T_0 can be understood as due to the formation of a large superzone gap originated from the AFM ordering [35], which leads to a rapid reduction in the density of conduction electron states at the Fermi energy. It is noteworthy that the increase in $\rho_{I\|a}(T)$, $\rho_{I\|b}(T)$, and $\rho_{I\|c}(T)$ continues until 1.8 K, the lowest temperature measured. This behavior is very different from that observed for $U_2Rh_3Si_5$, which reveals a small peak in $\rho_{I\|a'}(T)$ and $\rho_{I\|b}(T)$ curves just below T_N (=25 K, superzone-gap feature) followed by the continuous decrease, and this decrease behavior can be described by a small Fermi liquid term and the expression for a gapped spin-wave spectrum [1,23]. Comparing with $U_2Rh_3Si_5$, the superzone gap formed in $U_2Ir_3Si_5$ seems to be much larger than that formed in $U_2Rh_3Si_5$.

Another important feature of $U_2Ir_3Si_5$ disclosed in the present work is the two anomalies in the temperature dependences of magnetic susceptibility, specific heat, and electrical resistivity at T_N and T_0, which signify the second-order PM-AFM magnetic transition and the first-order phase transition, respectively. Note that similar double phase transitions have been observed for several other isostructural (or small monoclinic distortion from the $U_2Co_3Si_5$ structure) compounds of the "235" family, e.g., $Pr_2Pt_3Ge_5$ [8], $R_2Rh_3Si_5$ (R = Tb, Dy) [36], $Ce_2Ni_3Ge_5$ [37], $Tb_2Ni_3Si_5$ [38], and $Er_2Ni_3Si_5$ [39] etc. The transition appearing at the low-T side in these compounds also exhibits the first-order-like feature. We would like to point out that the first-order transition occurring at T_0 in $U_2Ir_3Si_5$ and other "235" compounds mentioned above seems to be due to the similar mechanism associated with some kind of structural variation around the transition temperature T_0. It should be emphasized that in the case of $U_2Rh_3Si_5$, specific-heat measurement indicates the first-order character of the PM-AFM transition at T_N [1], and neutron-diffraction results have confirmed that this transition is accompanied by an evident change in the lattice constants, as observed through the transition temperature [1,21]. Though this material forms with a monoclinic variation of $U_2Co_3Si_5$-type structure, it is quite likely that the similar mechanism is possible in our case of $U_2Ir_3Si_5$ and other "235" systems mentioned above.

Below T_0, what kind of magnetic state the system enters is a very interesting physical problem. Although there is currently no microscopic understanding of the low-T first-order phase transition, and the possibility of the system changing from the AFM-II state to another AFM state with different order parameters after the II-III phase transition cannot be ruled out, we would like to point out another possibility, that is, magnetic quadrupole ordering may exist below T_0. $U_2Ir_3Si_5$ and the above mentioned isostructural $R_2M_3X_5$ compounds have been confirmed to crystallize in an orthorhombic $U_2Co_3Si_5$-type crystal structure; the U (R) atoms in this structure form a quasi-1D zigzag chain along the c axis, which are well separated from the Ir-Si (M-X) ring. The zigzag chain of U (R) atoms is strongly coupled with the b axis through the Ir (M) atom [6]. As a result, local inversion symmetry at the U (R) site is broken, and odd parity multipole such as magnetic quadrupole may be induced [40–42]. Indeed, for $U_2Rh_3Si_5$, a quasiorthorhombic type (with a slight monoclinic distortion from the orthorhombic $U_2Co_3Si_5$ structure) system, the novel magnetic behaviors observed around the PM-AFM transition temperature T_N are related to a first-order phase transition into a simultaneous spin-quadrupolar ordering [1]. A similar mechanism may explain the first-order transition in $U_2Ir_3Si_5$ and other isostructural "235" compounds mentioned above. From this point of view, we cannot rule out the possibility of the existence of magnetic quadrupole ordering in $U_2Ir_3Si_5$ below T_0 at low magnetic field. Based on the present data, we cannot give a more detailed microscopic analysis on the magnetic structure of phase III (see Fig. 9). On the other hand, for a 1D antiferromagnetic spin system, it is well known that magnetic susceptibility can be calculated based on a suitable physical model such as the models of antiferromagnetic $S = 1/2$ and $S = 1$ Heisenberg spin chains [43–46], and the antiferromagnetic interchain coupling strength can be obtained by fitting the experimental data. Since the U atoms in $U_2Ir_3Si_5$ form a quasi-1D zigzag chain along the c axis, the similar thermodynamic analysis may be very meaningful for this system. To do this, we need more experimental information about the low-temperature spin structure to construct a corresponding physical model. Further experimental works such as neutron diffraction, NMR, thermal expansion, and resonant x-ray scattering will be very helpful to solve the above mentioned topics.

V. CONCLUSION

We have found a new compound, $U_2Ir_3Si_5$, and successfully grown its single crystal. This is the second successful example of single crystal growth of U-based "235" compounds to date. Our fundamental physical property measurements on the as-cast single crystalline $U_2Ir_3Si_5$ reveal the following

anomalous characteristics: (i) Double phase transitions occur at $T_N = 36$ K and $T_0 = 25.5$ K, respectively. The former represents a PM-AFM transition, and the latter displays the obvious characteristics of first-order phase transition. (ii) Electrical resistivity measurements reveal the negative TCR behavior, i.e., $d\rho/dT < 0$, for $I \parallel a$ and $I \parallel b$, which may be originated from the scattering of conduction electrons excited over the semiconductorlike narrow band gap or Kondo effect. (iii) Strong magnetic anisotropy is observed in the temperature and field dependences of susceptibility and high field magnetization. In particular, the high-field magnetization measured at 4.2 K for $H \parallel b$ shows three metamagnetic transitions around 200 kOe with a large hysteresis. In contrast, the $M(H)$ curve measured at 4.2 K for $H \parallel a$ and $H \parallel c$ does not reveal any anomaly up to 560 kOe. Based on these experimental results, a magnetic phase diagram of $U_2Ir_3Si_5$ is constructed. As one of the possibilities, the first-order transition at T_0 may be accompanied by the formation of magnetic quadrupole ordering due to the local symmetry breaking of the U site. Further experimental and theoretical works are necessary to verify this conjecture.

ACKNOWLEDGMENT

This work was financially supported by KAKENHI Grants No. JP15H05884, No. JP15H05882, No. JP16H04006, and No. JP15H05745.

[1] B. Becker, S. Ramakrishnan, A. A. Menovsky, G. J. Nieuwenhuys, and J. A. Mydosh, Phys. Rev. Lett. **78**, 1347 (1997).
[2] V. K. Anand, A. K. Nandy, S. K. Dhar, C. Geibel, and Z. Hossain, J. Magn. Magn. Mater. **313**, 164 (2007).
[3] Y. Muro, M. Nakano, and K. Motoya, J. Phys. Soc. Jpn. **77**, 124707 (2008), and references therein.
[4] Z. Hossain, H. Ohmoto, K. Umeo, F. Iga, T. Suzuki, T. Takabatake, N. Takamoto, and K. Kindo, Phys. Rev B **60**, 10383 (1999).
[5] S. Layek, V. K. Anand, and Z. Hossain, J. Magn. Magn. Mater. **321**, 3447 (2009).
[6] N. S. Sangeetha, A. Thamizhavel, C. V. Tomy, S. Basu, A. M. Awasthi, P. Rajak, S. Bhattacharyya, S. Ramakrishnan, and D. Pal, Phys. Rev. B **91**, 205131 (2015).
[7] M. Nakashima, H. Kohara, A. Thamizhavel, T. D. Matsuda, Y. Haga, M. Hedo, Y. Uwatoko, R. Settai, and Y. Onuki, J. Phys.: Condens. Matter **17**, 4539 (2005).
[8] N. H. Sung, C. J. Roh, K. S. Kim, and B. K. Cho, Phys. Rev B **86**, 224507 (2012).
[9] J. A. Gotaas, J. W. Lynn, R. N. Shelton, P. Klavins, and H. F. Braun, Phys. Rev. B **36**, 7277 (1987).
[10] V. K. Anand, Z. Hossain, and C. Geibel, Phys. Rev B **77**, 184407 (2008).
[11] J.-C. Griveau, E. Colineau, D. Bouëxiere, K. Gofryk, T. Klimczuk, and J. Rebizant, J. Alloys Compd. **576**, 409 (2013).
[12] E. D. Bauer, P. H. Tobash, J. N. Mitchell, J. A. Kennison, F. Ronning, B. L. Scott, and J. D. Thompson, J. Phys.: Condens. Matter **23**, 094223 (2011).
[13] E. Hickey, B. Chevalier, P. Gravereau, and J. Etourneau, J. Magn. Magn. Mater. **90–91**, 501 (1990).
[14] Y. Arita, K. Terao, S. Mitsuda, Y. Nishi, T. Matsui, and T. Nagasaki, J. Nucl. Mater. **294**, 206 (2001).
[15] L. Piraux, E. Grivei, B. Chevalier, P. Dordor, E. Marquestaut, and J. Etourneau, J. Magn. Magn. Mater. **128**, 313 (1993).
[16] P. Villars *et al.*, $U_2Mn_3Si_5$, in *Structure Types. Part 11: Space Groups (135) P42/mbc* (123) *P4/mmm*. Landolt-Börnstein - Group III Condensed Matter (Numerical Data and Functional Relationships in Science and Technology), Vol. 43A11, edited by P. Villars and K. Cenzual (Springer, Berlin, Heidelberg, 2012).
[17] F. Wastin, J. Rebizant, J. P. Sanchez, A. Blaise, J. Goffart, J. C. Spirlet, C. T. Walker, and J. Fuger, J. Alloys Compd. **210**, 83 (1994).
[18] Ya. P. Yarmolyuk, L. G. Aksel'rud, E. I. Gladyshevskii, and V. A. Bruskov, Sov. Phys. Crystallogr. **30**, 380 (1985).
[19] R. G. Leisure, S. Kern, F. R. Drymiotis, H. Ledbetter, A. Migliori, and J. A. Mydosh, Phys. Rev. Lett. **95**, 075506 (2005).
[20] T. Takeuchi, T. Yamada, Y. Miyako, K. Oda, K. Kindo, B. Becker, S. Ramakrishnan, A. A. Menovsky, G. J. Nieuwenhuys, and J. A. Mydosh, Phys. Rev B **56**, 10778 (1997).
[21] R. Feyerherm, C. R. Wiebe, B. D. Gaulin, M. F. Collins, B. Becker, R. W. A. Hendrikx, T. J. Gortenmulder, G. J. Nieuwenhuys, and J. A. Mydosh, Phys. Rev B **56**, 13693 (1997).
[22] F. Honda, D. X. Li, K. Okauchi, Y. Homma, A. Nakamura, and D. Aoki, MRS Advanves **1**, 2975 (2016).
[23] B. Becker, S. Ramakrishnan, S. Süllow, C. C. Mattheus, C. E. Snel, G. J. Nieuwenhuys, and A. Mydosh, Physica B **230–232**, 83 (1997).
[24] H. Y. Bai, C. Z. Tong, and P. Zheng, J. Appl. Phys. **95**, 1269 (2004).
[25] R. Tamura, T. Araki, and S. Takeuchi, Phys. Rev. Lett **90**, 226401 (2003).
[26] A. Pandey, C. Mazumdar, R. Ranganathan, M. De Raychaudhury, T. Saha-Dasgupta, S. Tripathi, D. Pandey, and S. Dattagupta, Europhys. Lett. **84**, 47007 (2008).
[27] J. M. Ziman, Philos. Mag. **6**, 1013 (1961).
[28] R. W. Cochrane, R. Harris, J. O. Ström-Olson, and M. J. Zuckermann, Phys. Rev. Lett. **35**, 676 (1975).
[29] P. J. Cote and L. V. Meisel, Phys. Rev. Lett. **39**, 102 (1977).
[30] U. Mizutani, *Introduction to the Electron Theory of Metals* (Cambridge University Press, Cambridge, 2003), Chap. 15.
[31] K. Gofryk, D. Kaczorowski, T. Plackowski, A. Leithe-Jasper, and Yu. Grin, Phys. Rev B **72**, 094409 (2005).
[32] K. Gofryk, D. Kaczorowski, T. Plackowski, J. Mucha, A. Leithe-Jasper, W. Schnelle, and Yu. Grin, Phys. Rev B **75**, 224426 (2007).
[33] R. Dornhaus, G. Nimitz, and B. Schlicht, *Narrow-Gap Semiconductors* (Springer, Berlin, 1983).
[34] J. Pierre and I. Karla, J. Magn. Magn. Mater. **217**, 74 (2000).

[35] A. R. Mackintosh, Phys. Rev. Lett. **9**, 90 (1962).
[36] S. Ramakrishnan, N. G. Patil, Aravind D. Chinchure, and V. R. Marathe, Phys. Rev. B **64**, 064514 (2001).
[37] Z. Hossain, S. Hamashima, K. Umeo, T. Takabatake, C. Geibel, and F. Steglich, Phys. Rev. B **62**, 8950 (2000).
[38] C. Mazumdar, K. Ghosh, R. Nagarajan, S. Ramakrishnan, B. D. Padalia, and L. C. Gupta, Phys. Rev. B **59**, 4215 (1999).
[39] C. Mazumdar, R. Nagarajan, A. K. Nigam, K. Ghosh, S. Ramakrishnan, L. C. Gupta, and B. D. Padalia, Physica B **339**, 216 (2003).
[40] L. Fu, Phys. Rev. Lett. **115**, 026401 (2015).
[41] S. Hayami, H. Kusunose, and Y. Motome, J. Phys. Soc. Jpn. **84**, 064717 (2015).
[42] S. Hayami, H. Kusunose, and Y. Motome, Phys. Rev. B **97**, 024414 (2018).
[43] D. C. Johnston, R. K. Kremer, M. Troyer, X. Wang, A. Klümper, S. L. Bud'ko, A. F. Panchula, and P. C. Canfield, Phys. Rev. B **61**, 9558 (2000), and references therein.
[44] J. C. Bonner, H. W. J. Blöte, J. W. Bray, and I. S. Jacobs, J. Appl. Phys. **50**, 1810 (1979).
[45] T. M. Rice, Z. Phys. B **103**, 165 (1997).
[46] F. D. M. Haldane, Phys. Rev. Lett. **50**, 1153 (1983), and references therein.